

Optical model potential analysis of $\bar{n}A$ and nA interactions

Teck-Ghee Lee¹ and Cheuk-Yin Wong²

¹*Department of Physics, Auburn University, Auburn, AL 36849, U.S.A. and*

²*Physics Division, Oak Ridge National Laboratory, Oak Ridge, TN 37831, U.S.A.*

We use a momentum-dependent optical model potential to analyze the annihilation cross sections of antineutron \bar{n} on C, Al, Fe, Cu, Ag, Sn, and Pb nuclei for projectile momenta $p_{\text{lab}} \lesssim 500$ MeV/ c . We obtain good description of annihilation cross sections data of Barbina *et al.* [Nucl. Phys. A **612**, 346 (1997)] and of Astrua *et al.* [Nucl. Phys. A **697**, 209 (2002)] which exhibit an interesting dependence of the cross sections on the p_{lab} as well as on the target atomic mass number A . We also obtain the neutron (n) non-elastic reaction cross sections for the same targets. Contrasting the nA reaction cross sections σ_{rec}^{nA} to the $\bar{n}A$ annihilation cross sections $\sigma_{\text{ann}}^{\bar{n}A}$, we find the $\sigma_{\text{ann}}^{\bar{n}A}$ is significantly larger than the σ_{rec}^{nA} , that is, the $\sigma_{\text{ann}}^{\bar{n}A}/\sigma_{\text{rec}}^{nA}$ cross section ratio lies between the values of order 1.8 and 3.8 in the momentum region where comparison is possible. The dependence of the annihilation cross section on the projectile charge is also examined in comparison with antiproton \bar{p} . Here we predict the $\bar{p}A$ annihilation cross section on the simplest assumption that both $\bar{p}A$ and $\bar{n}A$ interactions have the same nuclear part of the optical model potential but differs only on the electrostatic Coulomb interaction. Deviation from such simple model extrapolation in measurements will provide new information on the difference between $\bar{n}A$ and $\bar{p}A$ potentials.

PACS numbers: 24.10.-i, 25.43.+t, 25.75.-q,

I. INTRODUCTION

Annihilation between antinucleon and nucleon or nucleus defines one of the basic aspects in antimatter-matter interactions. Over the years there have been many experimental measurements [1–21] and theoretical analysis [21–41] about antinucleon annihilation on nucleon and nuclei. However, most of the work were carried out with antiproton \bar{p} projectile. Experimental and theoretical investigations using antineutron \bar{n} , on the other hand, are still relatively limited. Theoretical work have also been carried out on the relationship between $\bar{n}n$ oscillation and $\bar{n}A$ interaction potential [46–48]. Recently, it has also been suggested that $\bar{n}A$ annihilation can be used to prepare apparatus for the $\bar{n}n$ oscillations [49] detection.

On the experimental side, one representative investigation is the measurement of the \bar{n} -Fe annihilation cross section from 100 to 780 MeV/ c [42–45]. The experiment was carried out with LEAR facility at CERN in terms of $\bar{p}p \rightarrow \bar{n}n$ charge-exchange reaction. Another investigation is by the OBELIX group of Astrua *et al* [8], measured the annihilation cross sections of \bar{n} on C, Al, Cu, Ag, Sn, and Pb nuclei in the p_{lab} range from 50 to 400 MeV/ c . These experiments give a clear evidence about the dependence of antinucleon-nucleus absorption cross section on the atomic mass number A and the prominent absorption feature of inverse-momentum $1/p_{\text{lab}}$ dependence at low-energy. They are also useful to test the theories of antinucleon-nucleus interactions.

In response to the experimental efforts, Friedman derived an optical model potential for \bar{p} -nucleus interaction by accounting for both the neutron and proton densities [32] to examine the annihilation cross sections for \bar{p} and \bar{n} on all the six targets at seven energies studied in Astrua *et al* [8]. The calculated cross sections for \bar{p} and \bar{n} are compared with experimental annihilation cross sections for \bar{n} . The study indicated the \bar{p} induced annihilation cross sections increase much steeper in the low momenta $p_{\text{lab}} < 200$ MeV/ c region in comparison to the case for \bar{n} projectile. It also elucidated the larger \bar{p} annihilation cross sections match the experimental data closely, but surprisingly not for \bar{n} annihilation cross sections. Above 250 MeV/ c , the \bar{n} results are found to be reasonably close to the experimental cross sections. However, below 100 MeV/ c , the \bar{n} results are found to be significantly smaller than the experimental cross sections. Furthermore, the predicted \bar{n} annihilation cross sections appear to depreciate and shift to lower and lower momenta as the size of the nuclear target increases and thus deviate from the behavior suggested by the experimental cross sections. It is important to note that the very same density-folded optical model potential has been checked and tested previously, by the same author of Ref.[32], to reproduce very well the angular distributions for elastic scattering of \bar{p} by C, Ca and Pb at 300 MeV/ c [31].

The fact that \bar{n} induced annihilation cross sections is smaller than the \bar{p} can be easily understood in terms of the incoming electrically neutral projectile will naturally experience negligible Coulomb attraction from the target nucleus. But, the fact that experiment exemplified a notable absorption feature of $1/p_{\text{lab}}$ - type of dependence – akin to the effects of Coulomb focusing for \bar{n} annihilation cross sections at the lower momenta, and the microscopic optical potential predicted these cross sections being depreciated and shifted to lower and lower momenta as A increases are considerably perplexing!

Recently, we have extended the Glauber model for nucleus-nucleus collisions [50–53] to study the nuclear annihilation cross sections by antinucleons. The extended Glauber model for the calculation of the $\bar{p}A$ annihilation cross section [22, 23] considered the nucleon-nucleus collision as a collection of binary collisions, and took into account the appropriate shadowing and the inclusion of initial-state and in-medium interactions. The basic ingredients are the elementary $\bar{p}p$ and $\bar{p}n$ annihilation cross sections, $\sigma_{\text{ann}}^{\bar{p}p}$ and $\sigma_{\text{ann}}^{\bar{p}n}$, together with initial-state Coulomb interactions and the change of the momentum of the antinucleon inside the nuclear medium. We note that in our earlier study [22], the basic $\bar{p}p$ annihilation cross section, $\sigma_{\text{ann}}^{\bar{p}p}$, was parameterized semi-empirically as $1/v$, and employed in our investigation of the stability and the properties of matter-antimatter molecules [54, 55]. In our subsequent study [23], we improved the $\sigma_{\text{ann}}^{\bar{p}p}$ and $\sigma_{\text{ann}}^{\bar{p}n}$ formulas by considering the anti-particle transmission through a nuclear potential and the $\bar{p}p$ Coulomb interaction, the nuclear annihilation cross sections can be properly evaluated in a simple analytical form. The expressions are rigorous enough and therefore amend our earlier simple approach of $1/v$ function to parameterize the basic $\sigma_{\text{ann}}^{\bar{p}p}$ and $\sigma_{\text{ann}}^{\bar{p}n}$ cross sections. The strong absorption model formulated decomposes the incoming plane waves into a sum of partial waves of given orbital angular momentum L and assumes these partial waves transmit to the nucleon surface S leads to annihilation reaction. It is shown the cross sections for nuclear annihilation by \bar{p} and \bar{n} are simple functions of the momentum of the incident particles. Across the momenta range considered, contrasting it to the $\sigma_{\text{ann}}^{\bar{n}p}$ annihilation cross section, the $\sigma_{\text{ann}}^{\bar{p}p}$ annihilation cross section is significantly enhanced by the Coulomb interaction for the p_{lab} momenta of the incident particle below 500 MeV/ c . As the p_{lab} increases, the two annihilation cross sections become almost identical, approaching the Pomeranchuk’s equality limit [56] at $p_{\text{lab}} \sim 500$ MeV/ c . In addition, the calculated annihilation cross sections agree well with the experimental data. With the improved $\sigma_{\text{ann}}^{\bar{p}p}$ and $\sigma_{\text{ann}}^{\bar{p}n}$, we also reproduced the general map of annihilation cross sections, $\sigma_{\text{ann}}^{\bar{p}A}$, as a function nuclear mass numbers A and collision energies.

With encouraging results from the particle transmission theory to describe the $\sigma_{\text{ann}}^{\bar{p}p}$, $\sigma_{\text{ann}}^{\bar{p}n}$ and $\sigma_{\text{ann}}^{\bar{p}A}$ annihilation cross sections, we employed the very same theory to examine the $\sigma_{\text{ann}}^{\bar{n}A}$. But there was an inadvertent error rose through

the Coulomb trajectory modification considered in the extended Glauber model, making our $\sigma_{\text{ann}}^{\bar{n}A}$ to agree with the experiment data. We re-examined and re-evaluated our $\sigma_{\text{ann}}^{\bar{n}A}$ cross section, and found, in the absence of additional Coulomb effects, the rectified $\sigma_{\text{ann}}^{\bar{n}A}$ cross sections are significantly “flat” and relatively lower than the experimental data for $p_{\text{lab}} < 200$ MeV/ c , yielding a far from satisfactory agreement between our calculations and experiment of Astrua *et al.*

Anticipating new and better experiments [57–59] will be performed in the coming years, here we attempt to explore an alternative theoretical method to rectify our previous annihilation cross section results for $\bar{n}A$. Besides, it appears that a comparative study of the absorption cross sections induced by neutrons, antineutrons and antiprotons has not yet been made.

The content of this paper is as follows. In Section II, we present the phenomenological optical model potential (OMP) we obtained to examine the $\bar{n}A$ annihilation cross sections. In Section III, we assess our phenomenological theory by comparing our numerical results to the available experimental data. Finally, we conclude the present study with some discussions in Section VI.

II. PHENOMENOLOGICAL MOMENTUM-DEPENDENT OPTICAL MODEL POTENTIAL

The Glauber model is known to work best at high energies in which the extend individual nucleon can be treated as isolated scatterer. For low energies collisions, such description may not be as appropriate and the traditional optical model potential analysis be more suitable. For this reason we adopt a phenomenological OMP to analyze the energy-dependence $\bar{n}A$ annihilation cross section. Moreover, the method of OMP is well-tested and long-established for treating complicated interactions between an incoming nucleon and a nucleus [60, 61].

TABLE I. Antineutron optical model potential well depths, V'_o and $W_{(o,oD)}$, and the $b_{(0,1)}$ free parameters, are in MeV, and $V_D = 0$.

Nucleus	¹² C	²⁷ Al	⁵⁶ Fe	^{63.6} Cu	^{107.9} Ag	^{118.7} Sn	²⁰⁶ Pb
V'_o	56.00	56.00	56.00	60.00	82.00	90.00	90.00
W_o	22.03	22.03	22.03	25.33	23.70	27.03	27.03
W_{oD}	5.980	5.980	5.980	5.980	5.980	5.980	5.980
b_0	14.16	31.86	66.08	75.05	127.32	140.07	244.50
b_1	7.80	16.90	33.80	37.70	61.10	65.00	106.60

In the present analysis, we consider the collision between an antinucleon and a nuclei, and their effective interaction strength without spin-orbit interaction, is represented by a momentum-dependent optical model potential

$$U(r) = V_C(r) - V_V(r, p) - i(W_V(r, p) + W_D(r, p)), \quad (1)$$

where subscripts “V” and “D” denote the volume and surface terms, respectively; and

$$V_V(r, p) = V_o(p)f(r, r_V, a_V), \quad (2)$$

$$W_V(r, p) = W_o(p)f(r, r_W, a_W), \quad (3)$$

$$W_D(r, p) = -4a_{W_D}W_{oD}(p)\frac{d}{dr}f(r, r_{W_D}, a_{W_D}). \quad (4)$$

As usual the $f(r, r_x, a_x)$ form factor is a Wood-Saxon

$$f(r, r_x, a_x) = \frac{1}{1 + \exp[(r - r_x)/a_x]}, \quad (5)$$

where $x \equiv V, W, W_D$. The Coulomb term $V_C(r)$ is naturally zero for an electrically neutral projectile. Otherwise,

$$V_C(r) = \begin{cases} \frac{Z_A Z_p e^2}{2r_c} \left(3 - \frac{r^2}{r_c^2}\right) & \text{for } r \leq r_c, \\ \frac{Z_A Z_p e^2}{r} & \text{for } r > r_c, \end{cases} \quad (6)$$

for a charged projectile with Z_A and Z_p being the target and projectile nuclear charges, respectively, and $r_c = r_o A^{1/3}$ is the Coulomb radius with r_o being 1.25 fm.

Albeit our main focus here is the $\bar{n}A$'s optical model potential, our knowledge of $\bar{p}A$'s optical model potential is more extensive. To gain some intuitions about the shape and size of our desired OMP, knowledge of the $\bar{p}A$'s OMP is valuable as it could shed some light on the construction of $\bar{n}A$'s OMP. There are at least two families of the $\bar{p}A$ potential, and these families and their ambiguity have been studied by one of the present authors in [62]. One family, so-called S , has a much more shallow imaginary potential with W of order 15–45 MeV, associated with a deep real potential with V of order 200–350 MeV. The other one, so-called D , has a real well-depth V of order 100 MeV and a deep imaginary part W of order 100–200 MeV. On the other hand, the neutron-nucleus (nA) optical potential is also well-established. From Koning and Delaroche [61], we learned that the nA optical potential has a real well-depth V of the order of 60 MeV and considerably shallower imaginary potential with W of the order of 15 MeV for many nuclei across the periodic table, but with A -value greater than 23 u. This potential family is quite different from that of $\bar{p}A$.

The optical model potential of Koning and Delaroche has many advantages because of its simplicities and systematic variations. However, as it has not taken into account the effects of static and dynamical deformation of the nuclei, it has its limitations and its application to ^{12}C as we do here will exhibit an expected deficiency.

It is desirable to have a simple and “flexible”, and yet rich enough (*i.e.*, applicable in the very low momentum region) forms of optical model potential for $\bar{n}A$ that could also be useful to $\bar{p}A$ annihilation. We therefore concocted a momentum-dependent phenomenological optical model potential

$$V_o(p_{\text{lab}}) = V'_o \times \left(\frac{\cosh(\sqrt{(b_0 + p_{\text{lab}})} - \sqrt{b_0})}{\cosh(\sqrt{(b_1 + p_{\text{lab}})} - \sqrt{b_1})} \right), \quad (7)$$

where b_0 and b_1 are two adjustable parameters. Table I lists the optical model potential well depths and the two adjustable parameters used to describe the $\bar{n}A$ interaction.

TABLE II. Optical model potential parameters for antineutron- and neutron-nucleus, respectively. The neutron optical model potential parameters are from Ref.[61]. The geometry parameters r_x and diffusiveness parameters a_x are in fm. Note that $a_{V_D} = a_{W_D}$ and $V_D = 0$.

Nucleus	^{12}C	^{27}Al	^{56}Fe	^{64}Cu	^{108}Ag	^{119}Sn	^{206}Pb	
\bar{n}	r_V	1.653	1.785	1.653	2.000	1.764	1.705	1.882
	r_W	0.750	1.250	0.750	1.350	1.400	1.750	1.600
	r_{W_D}	1.260	1.260	1.260	1.260	1.260	1.260	1.260
	a_V	1.050	1.050	1.050	1.000	1.200	1.250	1.000
	a_W	0.850	0.850	0.850	0.900	1.200	1.200	1.500
	a_{W_D}	0.590	0.590	0.590	0.590	0.590	0.590	0.590
	n	r_V	1.127	1.162	1.186	1.203	1.219	1.221
r_W		1.127	1.162	1.186	1.203	1.219	1.221	1.235
r_{W_D}		1.306	1.290	1.282	1.279	1.267	1.264	1.249
a_V		0.676	0.665	0.663	0.668	0.662	0.660	0.647
a_W		0.676	0.665	0.663	0.668	0.662	0.660	0.647
a_{W_D}		0.543	0.538	0.532	0.534	0.527	0.525	0.510

In order to obtain the nA reaction cross section, we adopted the optical model potential by Koning-Delaroche [61]. To avoid later confusion, we shall call the antinucleon-nucleus scattering $U(r)$ with eq.(7) the phenomenological optical model potential (POMP). And we shall call the nA optical potential given in Ref.[61] the Koning-Delaroche's optical model potential (KD-OMP).

With these potentials, we solve the Schrödinger equation using the standard distorted wave approximation provided in the ECIS97 computer program [63] to obtain the scattering cross section. With individual target, we use a fixed value for V_o evaluated at $p_{\text{lab}} = 200$ MeV/ c for $p_{\text{lab}} \geq 200$ MeV/ c as V_o becomes almost monotonous in the high-energy range. Furthermore, we also check the sensitivity of the cross section at $p_{\text{lab}} = 200$ MeV/ c to the small variation ($\sim 5\%$) of V_o and made sure the changes in the cross section is less than 3 percents.

III. RESULTS AND DISCUSSION

In this section we first present a comparison of our $\bar{n}A$ annihilation cross section results with data from experimental measurements. Next, we examine the cross section ratios of the $\bar{n}A$ annihilation to nA reaction, and comment on their corresponding optical model potentials. We discuss the $\bar{p}A$ annihilation last.

A. $\bar{n}A$ annihilation cross sections in comparison with experiment

In our previous study [23], we have examined the $\bar{n}p$ annihilation cross section as a function of the antineutron momentum by considering the transmission through a nuclear potential. Although the annihilation cross section data for $\bar{n}p$ still remains rather sparse to date in comparison to $\bar{p}p$ and contain significant degrees of uncertainties, a good agreement is achieved between our theoretical results and experimental data from the OBELIX Collaboration [1] and from Brookhaven National Laboratory [2].

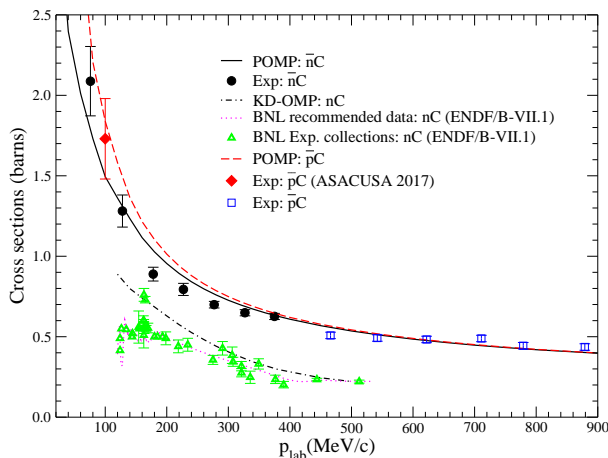


FIG. 1. (Color online) Comparison of $\bar{n}C$, $\bar{p}C$ annihilation cross sections and nC non-elastic reaction cross section as a function of the projectile momentum in the laboratory frame. The dash-dot-dotted line refers to nC reaction cross section obtained using KD-OMP; the dotted line and “ Δ ” are the nC reaction non-elastic data from Brookhaven National Laboratory’s National Nuclear Data Center [66].

A good way to verify and validate the present optical model potential model in describing the mass A and energy dependencies of \bar{n} annihilation (and of n reaction) is to check against the available experimental data.

In Fig. 1, we show a comparison of $\bar{n}C$ annihilation cross sections against several sets of data. Our predicted cross sections appear to quantitatively obey the energy dependence behavior suggested by the experiment at low momenta regime. As the p_{lab} increases above 500 MeV/c, the theoretical and experimental cross sections remain in good agreement with indication to depreciation in its energy dependence at large momenta.

It should be noted that in our calculations we assumed the $\bar{n}A$ annihilation potential has been produced by a uniformly charge distribution with reaction radius of $r_R = r_V A^{1/3}$. We considered this assumption is reasonable since it is well known that the $\bar{n}A$ annihilation cross section is approximately proportional to $A^{2/3}$ even at low momentum of ~ 60 MeV/c [7, 8] as the atomic mass number increases owing to the basic Glauber multiple collision process of the antineutron passing through a target of individual nucleons. Matching the cross section in term of πr_R^2 to the experimental antineutron-nucleus annihilation cross section, we can easily determine the OMP values for r_V by assuming $r_V = r_R$ for each nuclei. For example, even though the $\bar{n}C$ experimental annihilation cross section at p_{lab} 500 MeV/c is not readily available, but according to Pomeranchuk’s equality limit [56], at high energy both the $\bar{n}C$ and $\bar{p}C$ annihilation cross sections should be identical, therefore we use the experimental $\bar{p}C$ annihilation cross section of ~ 0.45 barns at 900 MeV/c to estimate our r_V to be 1.635 fm. The same assumption is considered for the rest of the targets. Table II contains the antineutron’s radial and diffuseness parameters as a function of atomic mass numbers. Fig. 7(a) illustrates the variation of V_o as a function of antineutron momentum. In general, they resemble the momentum functional form of $\sigma_{\text{ann}}^{\bar{n}A}$.

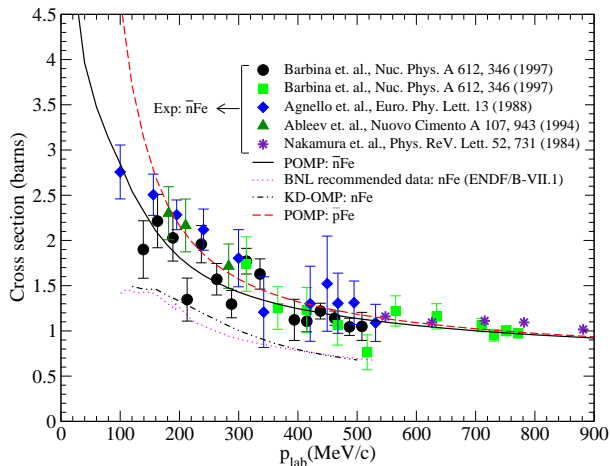


FIG. 2. (Color online) Comparison of $\bar{n}\text{Fe}$, $\bar{p}\text{Fe}$ annihilation cross sections and $n\text{Fe}$ non-elastic reaction cross section as a function of the projectile momentum in the laboratory frame. The symbols are experimental data of $\bar{n}\text{Fe}$ annihilation. The dash-dot-dotted line refers to $n\text{Fe}$ reaction cross section obtained using KD-OMP; the dotted line is the $n\text{Fe}$ reaction non-elastic data from Brookhaven National Laboratory’s National Nuclear Data Center [66].

In Fig. 2, we examine the $\bar{n}\text{Fe}$ annihilation cross sections along with several set of data. We ran some tests and found that the POMP geometrical parameters that are appropriate for $\bar{n}\text{C}$ annihilation also turned out to be appropriate for describing the $\bar{n}\text{Fe}$ interaction. The only variation we made is the potential strength V_o . For $p_{\text{lab}} > 40$ MeV/c, the $\bar{n}\text{Fe}$ interaction potential depth is about a factor of 2 shallower than the one of $\bar{n}\text{C}$ interaction. Otherwise, between the two potential strengths, they are not much different. The calculated $\bar{n}\text{Fe}$ annihilation cross sections also appeared to be in good agreement with the experimental data which indicate a much stronger absorption feature in comparison to the case of $\bar{n}\text{C}$ annihilation below p_{lab} of 400 MeV/c.

Fig. 3 displays how the $\bar{n}A$ annihilation cross sections depend on the nucleus mass number A . It is shown that at low momenta of $p_{\text{lab}} \lesssim 100$ MeV/c, the predicted $\bar{n}A$ annihilation cross sections for all targets, namely, Al, Cu, Ag, Sn and Pb, rise considerably as the projectile momentum keeps decreasing. They also fit quite well with the experimental data [8] in the momenta region where they exist. According to Fig. 3, we plotted the $\sigma_{\text{ann}}^{\bar{n}A}$ at $p_{\text{lab}} = 50$ and 100 MeV/c against their corresponding atomic mass number of $A^{2/3}$ in Fig. 4. The scattered points are the POMP predicted results. They are fitted with an expression of $\sigma_{\text{ann}}^{\bar{n}A} = \sigma_o A^{2/3}$. The fit is rather good. It clearly indicates the $\sigma_{\text{ann}}^{\bar{n}A}$ is indeed linearly depends on $A^{2/3}$. From optical models point of view, this means we have “black” nuclei and the annihilation occurs mainly on the surface of the nucleus.

Closely examining Fig. 4 also reveals the $\bar{n}\text{Fe}$ annihilation appears to somewhat deviate from this linear dependence. Perhaps future experiments could re-investigate this issue in the low momenta region where p_{lab} is less than 100 MeV/c.

In connection to the findings of Ref.[32], according to the evolution of $\sigma_{\text{ann}}^{\bar{n}A}$ cross sections as a function the nuclear mass number A displayed in Fig. 3, we do not notice any depreciation in and shifting of the $\sigma_{\text{ann}}^{\bar{n}A}$ cross sections to lower and lower momenta as the A value increases.

It is also informative to examine the inverse power law of $\bar{n}A$ annihilation. In the limit of low-energy, by parametrizing the theoretical annihilation cross section in an inverse power law form, $\sigma_{\text{ann}}^{\bar{n}A} \propto 1/p_{\text{lab}}^y$, in the range between 40 and 100 MeV/c, the y exponential value can be easily determined by setting $y = \partial \ln(\sigma_{\text{ann}}) / \partial \ln(p_{\text{lab}})$. Display in Fig. 5 gives the variation of y exponential values as a function of atomic mass number $A^{2/3}$. Taking an average over the 7 target nuclei yields a value of $y = 0.530$. This consequently suggests the $\sigma_{\text{ann}}^{\bar{n}A}$ may be proportional to $1/p_{\text{lab}}^{1/2}$ for target $A \geq 6$. This finding appears to be far from what we learned in our previous work [23]. There we found in the case of $\bar{n}p$, the exponential value $y = 1.08$ in the momentum range between 30 and 95 MeV/c. This exponential value is very close to the expected $y = 1.0$ value, a clear indication of the $1/p_{\text{lab}}$ behavior. Of course, in [23], the nuclear potential was assumed to be a constant there. Here, on the contrary, the nuclear optical potential depends on the projectile momentum, hence causing the $\sigma_{\bar{n}A}$ to deviate from the $1/p_{\text{lab}}$ law.

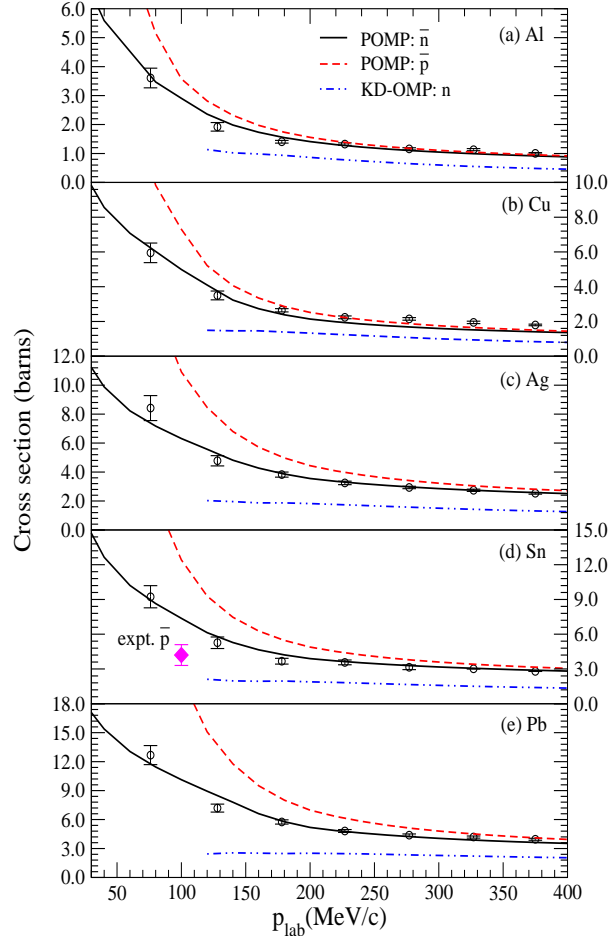


FIG. 3. (Color online) Cross sections for $\bar{n}A$, $\bar{p}A$ and nA , as a function of the projectile momentum in the laboratory frame. The solid line is for $\bar{n}A$, the dashed line is for $\bar{p}A$ and the dash-dot-dotted line is for nA . The opened circles are experimental data from Astrua *et al* [8]. The diamond is from Bianconi *et al* [9].

B. nA reaction cross sections

It is also of interest to compare the $\bar{n}A$ annihilation cross section against nA reaction cross section as a function of incoming projectile momenta. But before we do so, it is worthwhile to examine the quality of the present neutron reaction cross sections based on the KD-OMP. Displaying in Fig. 6 is a comparison between the present results and the BNL recommended non-elastic reaction cross section data for C, Al, Fe, Cu, Ag, Sn and Pb nuclei [66]. It is shown that the overall agreement between the calculated cross sections and recommended data is reasonably good.

Returning to Fig. 1 to 3, immediately become obvious is that all the $\sigma_{\text{ann}}^{\bar{n}A}$ annihilation cross sections are significantly larger than σ_{rec}^{nA} reaction cross sections. Let us first examine the cross section ratio of $\bar{n}C$ to nC interaction. At $p_{\text{lab}} = 100$ MeV/ c , the $\sigma_{\bar{n}C}/\sigma_{nC}$ ratio is found to be ~ 1.9 . On the other end, at higher $p_{\text{lab}} = 400$ MeV/ c , this ratio turns out to be ~ 1.8 . It is therefore safe to estimate, on average, this $\sigma_{\bar{n}C}/\sigma_{nC}$ ratio is close to 2 for p_{lab} between 100 and 400 MeV/ c where comparison is possible. Extrapolating to $p_{\text{lab}} = 900$ MeV/ c , the cross section ratio value appears to remain the same. It should be noted that in this low-energy regime we have assumed most of the nA non-elastic reaction owes to the absorption process. We further note that we restrict our analysis to the lowest momentum of 100 MeV/ c in order to avoid any complications from low-energy resonances.

We next look at the comparison between $\bar{n}Fe$ annihilation cross section and nFe non-elastic reaction cross section as a function of incoming projectile momenta. Similar to the case of $\sigma_{\bar{n}C}/\sigma_{nC}$ ratio, the $\sigma_{\bar{n}Fe}/\sigma_{nFe}$ ratio is also came out to be about 2 in the momenta range between 120 and 500 MeV/ c . As for the rest of the targets shown in Fig. 3, we find the $\sigma_{\text{ann}}^{\bar{n}A}/\sigma_{\text{rec}}^{nA}$ ratios turn out to be falling between the values of ~ 1.8 and 3.8 in the momenta range between 120 and 400 MeV/ c .

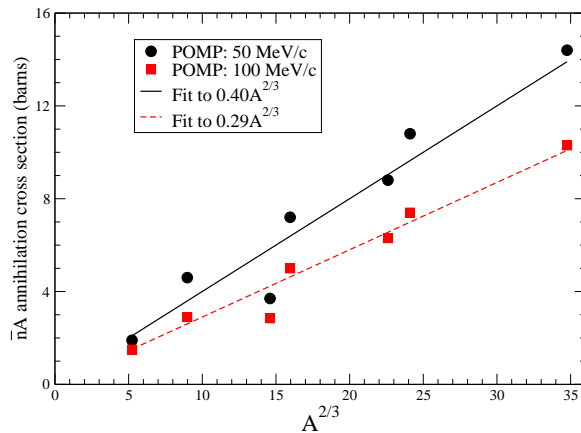


FIG. 4. (Color online) Antineutron annihilation cross sections as a function of atomic mass number $A^{2/3}$ at $p_{\text{lab}} = 50$ and 100 MeV/c, respectively.

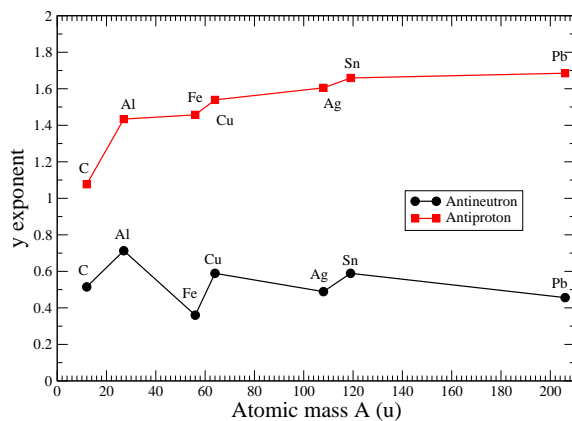


FIG. 5. (Color online) Exponential value, y , of $\bar{n}A$ and $\bar{p}A$, as a function of atomic mass number A .

Coming back to inspect the optical potential parameters for both $\bar{n}A$ and nA interactions. In Table I, the values of the initial potential depth V'_o at $p_{\text{lab}} = 20$ MeV/c for $\bar{n}A$ annihilation are comparable to that of the nA reaction for carbon and aluminum nuclei. The V'_o value increases to 90 MeV as A increases to 206 for lead. This trend is reversed according to the prescription of KD-OMP for nA reaction.

Fig. 7 displays the real part potential depth V_o as a function of momenta for $\bar{n}A$ and nA interactions. It is shown that the V_o of KD-OMP for nA reaction systematically decreases as a function of A values and in an almost linearly fashion as a function of projectile momenta in the range between 100 and 400 MeV/c. The variations of V_o from POMP for $\bar{n}A$, however, do not display such a trend and are almost momentum-independent in this momentum range. Moreover, for our corresponding imaginary parts, W_o and W_{oD} , are also quite different from that of the KD-OMP prescribed values. First of all, ours do not depend on the projectile momentum. Second, as shown in Table I, our W_o for $\bar{n}A$ increases from 22 to 27.03 MeV from carbon to lead nuclei. On the contrary, in the case of nA , Fig. 8(a) shows KD-OMP determined W_o decreases as a function of A and are less than 1.0 MeV at $p_{\text{lab}} = 100$ MeV/c. The W_o also increases as a function of momentum. Third, our W_{oD} for $\bar{n}A$ is fixed at 5.98 MeV for all targets. Conversely, the KD-OMP's W_o for nA do not. Their corresponding functional behaviors are shown in Fig. 8(b).

We next comment on the geometrical parameters, r_x , and diffusiveness parameters, a_x , for $\bar{n}A$ and nA interaction,

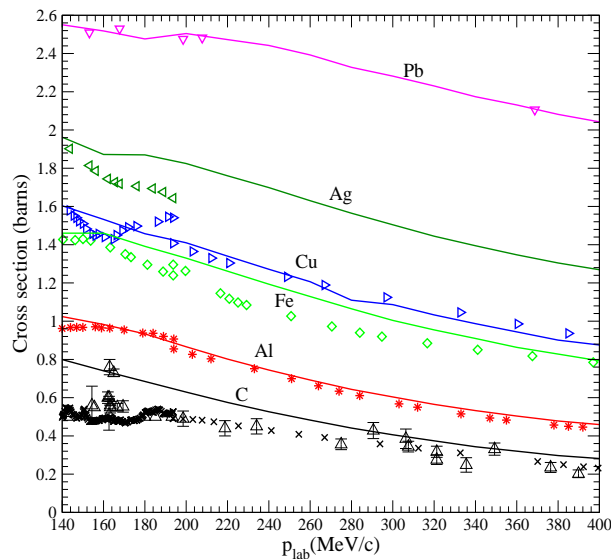


FIG. 6. (Color online) The nA non-elastic reaction cross section as a function of the projectile momentum in the laboratory frame. The solid-line refers to the present results obtained using the KD-OMP. The symbols are the data recommended by the Brookhaven National Laboratory's National Nuclear Data Center [66].

given in Table II. In the case of nA , the geometrical parameters $r_V = r_W$ show a systematic increase from 1.127 to 1.235 fm as the atomic mass number increases, whereas the r_{W_D} , on the other hand, shows a systematic decrease. And their corresponding $a_V = a_W$ and a_{W_D} diffusiveness parameters also follow the same manner. For the case of $\bar{n}A$ interaction, our geometrical and diffusiveness parameters, however, do not reflect such an order. In fact, we find $r_V \neq r_W$ and the r_V radii increases from 1.635 to 1.882 fm as A value increases from 12 to 206. That is, respectively, they are at least 40-50% larger than those of nA interaction. Moreover, the r_{W_D} radii is set to a constant value at 1.260 fm for the all nuclei. As for their corresponding diffusiveness parameters, $a_V \neq a_W$ and are notably larger compared to those of nA , and a_{W_D} are chosen to be a constant value of 0.590 fm as well. With these set of parameters, we find one could nicely match the theoretical cross section to the experimental data.

C. $\bar{p}A$ annihilation cross sections

As an adjunct to predicting the $\bar{n}A$ annihilation and nA reaction cross sections, we further predict the $\bar{p}A$ annihilation cross section in Fig. 1 to 3. We base our prediction on the simplest assumption that both $\bar{p}A$ and $\bar{n}A$ interactions have the same nuclear optical model potential but differs only on the long range Coulomb interaction. The goal is to examine the dependence of the annihilation cross sections on the projectile charge and to provide a benchmark for comparison against which the $\bar{n}A$ and $\bar{p}A$ interaction potentials may differ.

In comparison to neutral \bar{n} projectile, according to the annihilation cross sections displayed in Fig. 1 to 3, it is within our expectation that the charged \bar{p} projectile shows relatively larger annihilation cross section. In fact, because of the additional effects from Coulomb focusing, the \bar{p} annihilation cross sections for all the nuclei feature a steeper rise than that of $\bar{n}A$ interaction as the projectile momentum goes down. As the projectile momentum continues to increase, the effects from Coulomb focusing will also begin to diminish. As a result, the annihilation cross sections due to both \bar{n} and \bar{p} will eventually merge at $p_{\text{lab}} \sim 500$ MeV/ c , and finally reaches the Pomaranchuk's equality as their ratio comes to unity at 1.0 GeV/ c or so.

The plots also provide a clear evident about the $\bar{p}A$ annihilation cross sections do indeed vary with atomic mass A .

Recently, the ASACUSA's Collaboration took a new measurement for $\bar{p}C$ annihilation cross section at low energy of 5.3 MeV or $p_{\text{lab}} = 100$ MeV/ c [20]. Their cross section value of 1.73 ± 0.25 barns is also plotted in Fig. 1. Their datum clearly lies very close to our prediction.

Notice that in the case of $\bar{p}Sn$, we have also plotted the one and only experimental datum at 100 MeV/ c in Fig. 3 (d). The down side of this case is that there is no other comparable experimental measurements for \bar{p} and \bar{n} as in the case of proton. Therefore, for now, it is meaningless to make any comment on the energy dependence of the $\bar{p}Sn$

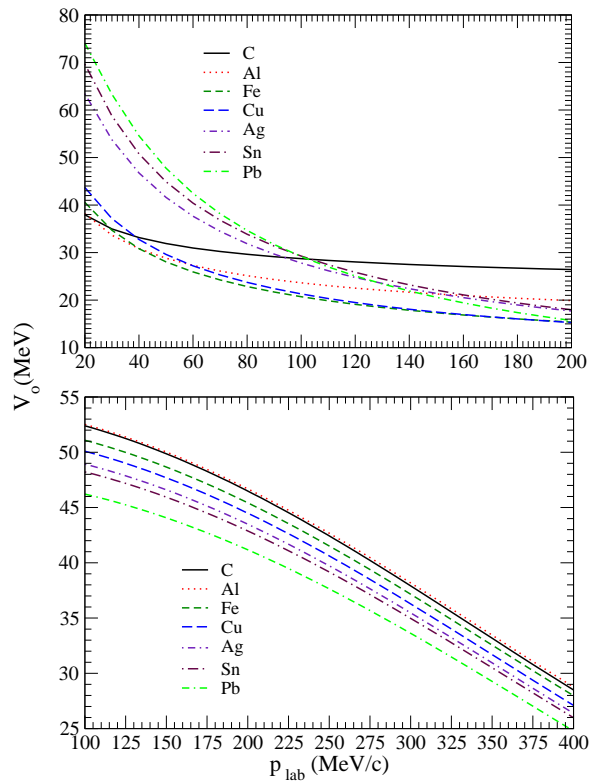


FIG. 7. (Color online) The variation of V_0 as a function of projectile momentum and atomic mass.

cross section.

As we have observed, at the low-energy limit, the slope for the $\bar{p}A$ interaction is much steeper in comparison to the $\bar{n}A$ one. So, it is also meaningful to analyze the inverse power law form, $\sigma_{\text{ann}}^{\bar{p}A} \propto 1/p_{\text{lab}}^y$, of $\bar{p}A$ annihilation. Similar to what we have discussed in the preceding section with respect to $\bar{n}A$ annihilation in Fig. 5, parametrizing the theoretical annihilation cross section in a power law form in the range between 40 and 100 MeV/c allows one to obtain the y exponential value. In our previous investigation [23] for the case of $\bar{p}p$, we have found that $y = 1.544$ in the momentum range between 30 and 50 MeV/c. Displayed in Fig. 5 is the variation of y as a function of atomic mass A . Similarly, averaging these values over the 7 nuclear targets yields a value of $y = 1.494$. As opposed to the case of $\bar{n}A$, this value is close to what we have found previously in the case of $\bar{p}p$ annihilation. This also means the Coulomb effect is predominant. Even though $y = 1.494$ is not quite equal to $y = 2.0$ as expected to be at the low-energy limit [64, 65], the behavior of the cross section is correctly approaching this limit as the projectile momentum keeps on decreasing. Therefore, this is sufficient to justify the $\sigma_{\text{ann}}^{\bar{p}A}$ is proportional to $1/p_{\text{lab}}^2$.

IV. SUMMARY AND CONCLUSIONS

The purpose of this contribution is in two folds. The first one is to revisit and rectify our previous annihilation cross section results for $\bar{n}A$ in [23]. The second one is to pursue a phenomenological analysis of \bar{n} annihilation cross section as a function of projectile momentum p_{lab} and atomic mass number A .

Previously, we have used the extended Glauber theory [23] to examine the experimental annihilation cross section data for \bar{n} on C, Al, Fe, Cu, Ag, Sn, and Pb in the momenta range below 500 MeV/c. But there was an inadvertent error rose through the Coulomb trajectory modification, causing the results to agree with the experimental data. After amending the theory, the re-evaluated results turned out to be in disagreement with the experiments.

The Glauber theory is well-known to valid for high-energy collisions in which the extend individual nucleon can be treated as isolated scatterer. It remains a good theoretical description for $p_{\text{lab}} \geq 200$ MeV/c. For low-energy collisions (*i.e.*, $p_{\text{lab}} < 200$ MeV/c), such description may not be as appropriate and the traditional optical model analysis be more

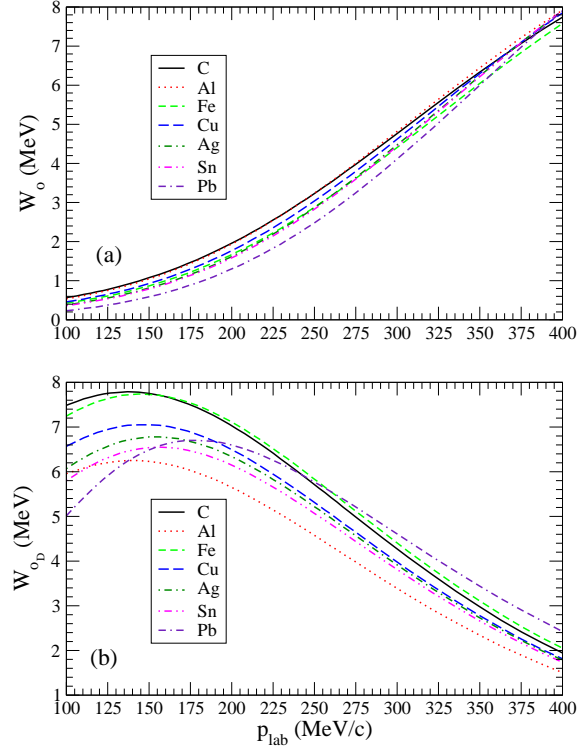


FIG. 8. (Color online) Neutron optical model potential well depth, $W_{(o,o_D)}$, as a function of projectile momentum.

suitable. For this reason we adopt the optical model potential to analyze the momentum-dependence $\bar{n}A$ annihilation cross section.

Inspired by the work of Friedman [31, 32] and Koning and Delaroche [61], we innovated a new form of momentum dependence optical model potential to describe $\bar{n}A$ interaction. Even though it is phenomenological and local, the momentum dependence of the present optical model potential in Eq.(7) is quite different from that of Koning-Delaroche and Friedman. The phenomenological optical model potential we concocted mimics the momentum dependence behavior displayed by the $\bar{n}A$ annihilation cross section. Yet it is rudimentary as well as comprehensive enough to treat the very low-momentum $\bar{n}A$ annihilation. Furthermore, it has the flexibility to describe the $\bar{p}A$ annihilation as well. Of course, in the future, with an extensive set of different experimental observables, one will be able to improve upon such “initial” optical model potential.

We employed the momentum dependence optical model potential in the Schrödinger equation and it’s solved within the standard distorted wave approximation provided in the ECIS97 computer program [63] to evaluate and analyze the annihilation cross sections for $\bar{n}A$ and $\bar{p}A$. We have also made use of Koning-Delaroche momentum dependence optical model potential to examine the nA non-elastic reaction cross section as a function of projectile momentum.

Although the present $\bar{n}A$ annihilation cross section show agreement with the experimental data, this does not mean that we have fundamentally understood this neutral $\bar{n}A$ annihilation mechanism. In fact, we are exactly on the opposite. For a start, why is the $\sigma_{\text{ann}}^{\bar{n}A}/\sigma_{\text{rec}}^{nA}$ cross section ratio appears to be so large? From a simple geometrical argument, in comparison to the incoming neutron n , why the antineutron \bar{n} seems to have a larger “influential” area for the target nucleus to react?

We have also demonstrated and verified that the $\sigma_{\text{ann}}^{\bar{n}A}$ is indeed approximately proportional to $A^{2/3}$ in the low-momentum region. Furthermore, we have illustrated that, in the low-energy limit, for the neutral or Coulomb-free $\bar{n}A$ interactions, the annihilation $\sigma_{\text{ann}}^{\bar{n}A} \propto 1/p_{\text{lab}}$. On the contrary, for a charged $\bar{p}A$ interactions, due to the combined effects from nuclear and Coulomb interactions, the annihilation $\sigma_{\text{ann}}^{\bar{p}A} \propto 1/p_{\text{lab}}^2$. In conclusion, we have calculated the $\bar{n}A$ annihilation cross section based on the simplest assumption that both $\bar{n}A$ and $\bar{p}A$ interactions have the same nuclear optical potential but differs only on the long-range electrostatic interaction. Any deviation from such simple

model extrapolation in measurements will shed new information on the difference between $\bar{n}A$ and $\bar{p}A$ potentials.

Acknowledgment

The authors thank Drs. Yuri Kamyshkov and Luca Venturelli for helpful discussions and communications. The research was supported in part by the Division of Nuclear Physics, U.S. Department of Energy under Contract DE-AC05-00OR22725.

-
- [1] A. Bertin, *et al.*, Nucl. Phys. B (Proc. Suppl.) **56A**, 227 (1997).
 - [2] T. Armstrong *et al.*, Phys. Rev. D **36**, 659 (1987).
 - [3] W. Brückner, *et al.*, Z. Phys. A **335**, 217 (1990).
 - [4] A. Bertin, *et al.*, OBELIX Collaboration, Phys. Lett. B **369**, 77 (1996).
 - [5] A. Benedettini, *et al.*, Nucl. Phys. B (Proc. Suppl.) **56A**, 58 (1997).
 - [6] A. Zenoni, *et al.*, OBELIX Collaboration, Phys. Lett. B **461**, 405 (1999).
 - [7] F. Iazzi, *et al.*, Phys. Lett. B **475** 378 (2000)
 - [8] M. Astrua, *et al.*, Nucl. Phys. A **697**, 209 (2002)
 - [9] A. Bianconi, *et al.*, Phys. Lett. B **704** 461 (2011).
 - [10] A. Bianconi, *et al.*, Phys. Lett. B **481**, 194 (2000).
 - [11] A. Bianconi, *et al.*, Phys. Lett. B **492**, 254 (2000).
 - [12] T. R. Bizzarri, *et al.*, Nuovo Cim. A **22**, 225 (1974).
 - [13] A. Zenoni, *et al.*, OBELIX Collaboration, Phys. Lett. B **461**, 413 (1999).
 - [14] F. Balestra, *et al.*, Phys. Lett. B **230**, 36 (1989).
 - [15] F. Balestra, *et al.*, Phys. Lett. B **149**, 69 (1984).
 - [16] F. Balestra, *et al.*, Phys. Lett. B **165**, 265 (1985).
 - [17] K. Nakamura, *et al.*, Phys. Rev. Lett. **52**, 731 (1984).
 - [18] F. Balestra, *et al.*, Nucl. Phys. A **452**, 573 (1986).
 - [19] V. Ashford, *et al.*, Phys. Rev. C **31**, 663 (1985).
 - [20] H. Aghai-Khozani *et al.*, Nucl. Phys. A **970**, 366 (2018).
 - [21] E. Klempt, C. Batty and J.-M. Richard, Phys. Rep. **413**, 197 (2005).
 - [22] T. G. Lee and C. Y. Wong, Phys. Rev. C **89**, 054601 (2014).
 - [23] T. G. Lee and C. Y. Wong, Phys. Rev. C **93**, 014616 (2016).
 - [24] J. Mahalanabis, *et al.*, Nucl. Phys. A **485**, 546 (1988).
 - [25] V. F. Kuzichev, Yu. B. Lepikhin and V. A. Smirnitsky., Nucl. Phys. A **576**, 581 (1994).
 - [26] J. Carbonell and K. Protasov, Hyperfine Interact. **76**, 327 (1993)
 - [27] J. Carbonell, K. Protasov and A. Zenoni, Phys. Lett. B. **397**, 345 (1997)
 - [28] A. Bianconi, *et al.*, Phys. Rev. C **62**, 014611 (2000).
 - [29] A. Gal, E. Friedman and C. J. Batty, Phys. Lett. B **491**, 219 (2000).
 - [30] C.J. Batty, E. Friedman and A. Gal, Nucl. Phys. A. **689**, 721 (2001).
 - [31] E. Friedman, Nucl. Phys. A **925**, 141 (2014).
 - [32] E. Friedman, Hyperfine Interact **234**, 77-84 (2015).
 - [33] V.V. Uzhinsky and A.S. Galoyan, arXiv:hep-ph/0212369.
 - [34] A.S.Galoyan and A.Polanski, arXiv:hep-ph/0304196.
 - [35] A. Galoyan, J. Ritman, A. Sokolov and V. Uzhinsky, arXiv:0809.3804.
 - [36] A.S. Galoyan and V.V. Uzhinsky, JETP Lett. **94**, 499 (2011); Pisma Zh . Eksp . Teor . Fiz. **94** (2011) 539 DOI: 10.1134/S0021364011190076.
 - [37] V. Uzhinsky, J. Apostolakis, A. Galoyan, *et al.*, Phys. Lett., B **705**, 235 (2011).
 - [38] A. Galoyan and V. Uzhinsky, arXiv:1208.3614.
 - [39] A. Galoyan *et al.*, Hyperfine Interact. **215**, 1-3, 69-76 (2013) DOI: 10.1007/s10751-013-0780-2
 - [40] A. Galoyan, PANDA Collaboration Report (B.P. Singh (Aligarh Muslim U.) *et al.*). Sep 2, 2014. 16 pp., e-Print: arXiv:1409.0865 [hep-ex]
 - [41] A. Galoyan, PoS Baldin ISHEPP XXII 049 (2015).
 - [42] M. Agnello *et al.*, Eur. Phys. Lett., **7**, 13 (1988).
 - [43] C. Barbina *et al.*, Nucl. Phys. A **612**, 346 (1997).
 - [44] K. Nakamura *et al.*, Phys. Rev. Lett. **52**, 731 (1984).
 - [45] V. G. Ableev *et al.*, Nuovo Cimento A **107**, 943 (1994).
 - [46] C. B. Dover, A. Gal, and J. M. Richard, Phys. Rev. D **27**, 1090 (1983); Phys. Rev. C **31**, 1423 (1985); Nucl. Instrum. Methods Phys. Res., Sect. A **284**, 13 (1989).
 - [47] L. A. Kondratyuk JETP. Lett. **64**, 495 (1996)
 - [48] E. Friedman and A. Gal., Phys. Rev. D **78**, 016002 (2008).
 - [49] D. G. Phillips *et al.*, Physics Reports **612**, 1 (2016)
 - [50] R. J. Glauber, in Lectures in Theoretical Physics, edited by W. E. Brittin and L. G. Dunham (Interscience, N. Y., 1959), Vol 1, p. 315.

- [51] R. Glauber and G. Matthiae, Nucl. Phys. B **21**, 135 (1970).
- [52] C. Y. Wong, Phys. Rev. D **30**, 961 (1984).
- [53] C. Y. Wong, *Introduction to High-Energy Heavy-Ion Collisions*, World Scientific Publisher, 1994.
- [54] C. Y. Wong and T. G. Lee, Ann. Phys. **326**, 2138 (2011).
- [55] T. G. Lee, C. Y. Wong and L. S. Wang, Chin. Phys. **17** 2897 (2008).
- [56] I. Pomeranchuk, JETP **30**, 423 (1956)
- [57] *FAIR - Facility for Antiproton and Ion Research*, Green Paper, October 2009.
- [58] W. Erni *et al.*, (PANDA Collaboration), Euro. Phys. Jour. A **49**, 25 (2013).
- [59] S. Maury, (for the AD Team), *the Antiproton Decelerator (AD)*, CERN/PS 99-50 (HP) (1999).
- [60] R.L. Varner, W.J. Thompson, T.L. McAbee, E.J. Ludwig, T.B. Clegg, Phys. Rep. 201 (1991) 57.
- [61] A. J. Koning and J. P. Delaroche, Nucl. Phys. A **713**, 231 (2003)
- [62] C. Y. Wong, A. K. Kerman, G. R. Satchler and A. D. MacKellar, Phys. Rev. C **29**, 574 (1984).
- [63] J. Raynal, Phys. Rev. C **23**, 2571 (1981); ECIS97 (<https://people.nsl.msui.edu/~brown/reaction-codes/home.html>)
- [64] E.P. Wigner, Phys. Rev. **73**, 1002 (1948).
- [65] L. D. Landau and E. M. Lifshitz, *Quantum Mechanics* (Pergamon, Oxford 1958).
- [66] Brookhaven National Laboratory, National Nuclear Data Center (www.nndc.bnl.gov/sigma/index.jsp)